CDDpress

www.nature.com/cdd

ARTICLE

Check for updates

Human cytomegalovirus hijacks host stress response fueling replication stress and genome instability

Joanna Maria Merchut-Maya[1,2], Jiri Bartek Jr[1,3,4,5], Jirina Bartkova[1,6], Panagiotis Galanos[1], Mattia Russel Pantalone[3,7], MyungHee Lee[1,2], Huanhuan L. Cui[3], Patrick J. Shilling[8], Christian Beltoft Brøchner[9], Helle Broholm[9], Apolinar Maya-Mendoza[1,2]✉, Cecilia Söderberg-Naucler[3,7,10,11]✉ and Jiri Bartek[1,6,12]✉

Viral infections enhance cancer risk and threaten host genome integrity. Although human cytomegalovirus (HCMV) proteins have been detected in a wide spectrum of human malignancies and HCMV infections have been implicated in tumorigenesis, the underlying mechanisms remain poorly understood. Here, we employed a range of experimental approaches, including single-molecule DNA fiber analysis, and showed that infection by any of the four commonly used HCMV strains: AD169, Towne, TB40E or VR1814 induced replication stress (RS), as documented by host-cell replication fork asymmetry and formation of 53BP1 foci. The HCMV-evoked RS triggered an ensuing host DNA damage response (DDR) and chromosomal instability in both permissive and non-permissive human cells, the latter being particularly relevant in the context of tumorigenesis, as such cells can survive and proliferate after HCMV infection. The viral major immediate early enhancer and promoter (MIEP) that controls expression of the viral genes *IE72* (IE-1) and *IE86* (IE-2), contains transcription-factor binding sites shared by promoters of cellular stress-response genes. We found that DNA damaging insults, including those relevant for cancer therapy, enhanced *IE72/86* expression. Thus, MIEP has been evolutionary shaped to exploit host DDR. Ectopically expressed IE72 and IE86 also induced RS and increased genomic instability. Of clinical relevance, we show that undergoing standard-of-care genotoxic radio-chemotherapy in patients with HCMV-positive glioblastomas correlated with elevated HCMV protein markers after tumor recurrence. Collectively, these results are consistent with our proposed concept of HCMV hijacking transcription-factor binding sites shared with host stress-response genes. We present a model to explain the potential oncomodulatory effects of HCMV infections through enhanced replication stress, subverted DNA damage response and induced genomic instability.

Cell Death & Differentiation (2022) 29:1639–1653; https://doi.org/10.1038/s41418-022-00953-w

INTRODUCTION

Epidemiological and experimental evidence implicates viral infections, particularly by papillomaviruses and hepatitis B and C viruses, as cancer-causing agents, implying that behind tobacco, viruses represent one of the most prevalent risk factors for cancer [1]. Additional viruses that are being scrutinized for their emerging links with cancer include the human cytomegalovirus (HCMV) that latently infects the majority of the human population, with 90% seroprevalence in the World Health Organization (WHO) Eastern Mediterranean region and 66% in the WHO European region [2]. After a primary infection, HCMV is carried asymptomatically in healthy individuals for the rest of their lives, but it can be lethal for immunocompromised patients who reactivate the virus or become reinfected. HCMV infection is also a leading cause of congenital malformations, resulting in neurodevelopmental delay, hearing loss and fetal or neonatal death [3]. Expression of HCMV proteins has been reported in multiple types of human malignancies [4, 5], but the significance of their presence and relationship with cell transformation are not well understood. Detection of HCMV in brain tumors, including glioblastoma multiforme (GBM) [6–8], is consistent with reports that anti-HCMV treatment combined with standard therapy extends survival of patients with GBM [9, 10]. Also, for unexplained reasons, HCMV is frequently reactivated upon radio-chemotherapy in brain tumor patients, which leads to encephalitis and is associated with poor patient outcome [11, 12].

HCMV is one of the herpesviruses reported to induce the host-cell DNA damage response (DDR) in permissive cells and subvert it to perform aberrant functions, beneficial for replication of the viral genome. Upon infection, several DDR proteins are upregulated

[1]Genome Integrity, Danish Cancer Society Research Center, Copenhagen, Denmark. [2]DNA Replication and Cancer Group, Danish Cancer Society Research Center, Copenhagen, Denmark. [3]Department of Medicine, Unit of Microbial Pathogenesis, Karolinska Institutet, Stockholm, Sweden. [4]Department of Neurosurgery, Karolinska University Hospital, Stockholm, Sweden. [5]Department of Neurosurgery, Copenhagen University Hospital Rigshospitalet, Copenhagen, Denmark. [6]Department of Medical Biochemistry and Biophysics, Division of Genome Biology, Science for Life Laboratory, Karolinska Institute, Stockholm, Sweden. [7]Department of Neurology, Karolinska University Hospital, Stockholm, Sweden. [8]Department of Biochemistry and Biophysics, Stockholm University, Stockholm, Sweden. [9]Department of Pathology, Copenhagen University Hospital Rigshospitalet, Copenhagen, Denmark. [10]MediCity Research Laboratory, University of Turku, Turku, Finland. [11]Institute of Biomedicine, University of Turku, Turku, Finland. [12]Genome Integrity Laboratory, Institute of Molecular Genetics, Prague, Czech Republic. ✉email: apomm@cancer.dk; cecilia.naucler@ki.se; jb@cancer.dk

Edited by G Melino

Received: 9 July 2021 Revised: 3 February 2022 Accepted: 3 February 2022
Published online: 22 February 2022

and some are localized in viral replication compartments (VRC) [13, 14]. Therefore, it has been suggested that these DDR factors might be exploited by the virus to proofread and resolve its genome before virion assembly. Among those, activated ATM kinase has been reported to contribute to efficient HCMV DNA replication [15]. The DNA damage binding protein 2 (DDB2), which is a component of the nucleotide excision repair (NER) pathway, induces ATM accumulation, while ATM decreases DDB2 expression. This negative feedback loop might be important for HCMV replication and virion production, as DDB2 deficiency reduced expression of genes associated with lytic origin firing and impaired production of infectious particles [16]. The role of DDR in HCMV replication remains, however, debatable as other studies suggest that neither ATM nor Mre11 is required for viral replication and virion production [13, 17]. Some DDR proteins have also been shown to be mislocalized from the nucleus to the cytoplasm upon infection, preventing checkpoint signaling and inhibiting host DDR [18, 19]. While intriguing, the significance and the mechanism of DDR subversion by HCMV, and their potential links with oncogenesis remain elusive, especially in non-permissive cells that can survive the infection and carry the virus latently. Our experiments and results presented below address some of these open questions in an attempt to better understand the oncomodulatory potential of HCMV infection and its relevance for human glioblastoma pathogenesis and therapy.

MATERIALS AND METHODS

Cell culture, viral infection and drug treatment

Human BJ normal skin fibroblasts (ATCC®CRL-2522™, male), MRC-5 normal lung fibroblasts (ATCC®CCL-171™, male), MCF-7 breast adenocarcinoma (ATCC®HTB-22™, female), HCT116 colorectal carcinoma (ATCC®CCL-247™, male), T98G glioblastoma multiforme (ATCC®CRL-1690™, male) and U-2 OS osteosarcoma (ATCC®HTB-96™, female) cell lines were cultured at 37 °C 5% CO_2 in Dulbecco's Modified Eagle Medium (DMEM) (Gibco, Carlsbad, CA USA) supplemented with 10% Fetal Bovine Serum (FBS) (Gibco) and penicillin/streptomycin (Gibco). U-2 OS and BJ Myc-ER stable cell lines overexpressing the fusion protein MycER under a constitutive promoter, and BJ cells with doxycycline-inducible expression of H-Ras (Lenti-X™ Tet-On Advanced Inducible Expression System, Clontech, Mountain View, Ca. USA) were generated previously in our laboratory [20]. Infection of non-synchronized cells with HCMV AD169, Towne, TB40E or VR1814 strains was performed at 37 °C 5% CO_2 in DMEM with 2% FBS for 1 h, after which cells were washed twice with low-FBS DMEM and grown in low-FBS DMEM for different times post-infection. Inactivation of HCMV strains was performed by treating viral stocks with the UV-C light in a UV lightbox apparatus for 10 min. Cells were treated with different concentrations of the following drugs: neocarzinostatin (NCS; Sigma–Aldrich, Darmstadt, Germany), cisplatin (Hospira, Lake Forest, Illinois, USA), temozolomide (TMZ; Sigma–Aldrich), aphidicolin (aphi; Sigma–Aldrich), Actinomycin D (AD; Sigma–Aldrich), THZ1 (CDK7i; APExBIO), Tumor Necrosis Factor α (TNFα; Sigma–Aldrich), ganciclovir (Sigma–Aldrich).

Immunofluorescence

Cells grown on coverslips were fixed with 4% cold formaldehyde (VWR Chemicals) (10 min, room temperature (RT)), permeabilized with 0.5% Triton X-100 (Merck) in Phosphate-buffered Saline (PBS) (Gibco) (10 min, RT) and blocked in PBS containing 0.1% Tween® 20 and 1% Bovine Serum Albumin (BSA) (Sigma–Aldrich) (15 min, RT). Cells were then incubated with primary antibodies for 1 h at RT, washed with PBS and stained with goat anti-rabbit, anti-mouse, anti-rat or anti-human AlexaFluor-488, -568 or -647 secondary antibodies (Invitrogen) for 45 min at RT. Cell nuclei were visualized using Hoechst 33342 (Invitrogen) in PBS (5 min, RT). Finally, coverslips were washed with PBS and ddH_2O, air-dried and mounted with the ProLong Gold Antifade Reagent (Life Technologies). Images were acquired using the LSM700 or LSM800 confocal microscope (Carl Zeiss, Oberkochen, Germany), the 63x/1.4 oil immersion or 20x objective (Carl Zeiss) and LSM ZEN software. Image analysis was performed using ImageJ software. For the analysis of nuclear proteins, a sub-mask of the nuclear area using DNA staining was created, the area recorded, added to the manager and the intensity of the signal in that area from the next color channel was measured. The intensity of the antibody signal in the cytoplasm was scored manually by detecting mean intensity in specific areas of the cytoplasm. Presented results are from 2–5 independent experiments. Primary antibodies used were: IE72/86 (MAB810R, Millipore; mouse, 1:500), IE86 (sc-69835, Santa Cruz; mouse, 1:500), ICP36 (UL44; CA006-100, Virusys Corporation; mouse, 1:500), γH2AX (ab22551, Abcam; mouse, 1:1000), 53BP1 (sc-22760, Santa Cruz; rabbit, 1:500), RPA32 S4/8 (A300-245A, Bethyl; rabbit, 1:200), p65 (ab32536, Abcam; rabbit, 1:500), α-tyrosinated tubulin (MCA77G, Bio-Rad; rat, 1:500), Centromere Protein (15-235-0001, Antibodies Inc.; human, 1:500).

Plaque assay

MRC-5 fibroblasts were seeded in 24-well plates and inoculated when cells reached confluence. Each well was inoculated with 200 µl of the virus-containing medium with serial dilution from 10^{-2} to 10^{-7}. After 90 min of adsorption, the medium was removed and wells were overlaid with 0.2% agarose in MEM medium supplemented with 5% FBS, 2 mM L-glutamine and penicillin/streptomycin. Plates were incubated for 14 days at 37 °C, 5% CO_2.

Immunoblotting

Cell lysates were prepared at different time post-infection using a hot (95 °C) Laemmli sample buffer (50 mM Tris pH 6.8, 2% SDS, 10% glycerol, 1% β-mercaptoethanol, 50 mM EDTA, 0.1% bromophenol blue in ddH_2O). Proteins were separated using the Novex NuPAGE SDS-PAGE system (ThermoFisher Scientific, Waltham, MA USA) according to the manufacturer's instructions and transferred to nitrocellulose membranes (GE Healthcare) using the iBlot blotting system (ThermoFisher Scientific) according to the manufacturer's instructions. Membranes were blocked in a blocking buffer (5% dry milk, 0.1% Tween® 20 in PBS) and incubated with primary antibodies diluted in the blocking buffer at 4 °C overnight. After incubation for 1 h at RT with HRP-conjugated anti-rabbit or anti-mouse secondary antibodies (PI-1000 and PI-2000, Vector Laboratories) diluted in the blocking buffer, proteins were detected using ECL detection reagents (GE Healthcare). Primary antibodies used were: IE72/86, IE86, γH2AX, 53BP1, p53 (sc-6243, Santa Cruz; rabbit), p21 (sc-756, Santa Cruz; rabbit), PCNA (sc-56, Santa Cruz; mouse), DNA Ligase 1 (ab177946, Abcam; rabbit), Fen1 (ab23828, Abcam; rabbit), fibrillarin (ab5821, Abcam; rabbit), RNF168 (rabbit polyclonal antibody provided by D. Durocher (The Lunenfeld-Tanenbaum Research Institute, Toronto, Canada)), DHX9 (A300-855A, Bethyl; rabbit), Cyclin E (ab3927, Abcam; mouse), SP1 (07-645, Upstate; rabbit), p65, p38 MAPK total (9212, Cell Signaling; rabbit), phospho-p38 MAPK (9215, Cell Signaling; rabbit), GFP (AB3080P, Millipore; rabbit), GAPDH (GTX627408, GeneTex; mouse), β-actin (A1978, Sigma–Aldrich; mouse), α-tubulin (sc-8035, Santa Cruz; mouse).

Immunohistochemistry

To detect HCMV immediate early and late antigen proteins in human primary and recurrent glioblastoma specimens, we employed our well-established sensitive immunohistochemical staining protocol [21]. Standard deparaffinization of the archival formalin-fixed, paraffin-embedded tissue sections was followed by antigen unmasking in the Tris/EDTA buffer (pH 9, 15 min microwave exposure). After overnight incubation with primary antibodies (mouse monoclonal antibody to HCMV immediate early protein (Millipore, MAB810R; 1:2000); mouse monoclonal antibody to HCMV late antigen protein (Millipore, MAB8127; 1:1000)), samples were processed for the indirect streptavidin-biotin-peroxidase method using the Vectastain Elite kit (Vector Laboratories) and nickel-sulfate-based chromogen enhancement detection, as described previously, without nuclear counterstaining [21]. For negative controls, sections were incubated with non-immune murine serum; for positive controls, a mouse monoclonal antibody to human phospho-histone H2A.X (Ser 139) (Millipore, clone JBW 301, diluted 1:2500) was used. The results were evaluated by two experienced researchers, including a senior oncopathologist, and the data expressed in scoring categories based on the percentage of positive tumor cells expressing the respective HCMV protein (see examples of staining patterns in Fig. 6F). Immunohistochemistry images were analyzed using Fiji software. The image threshold was adjusted equally and positive staining was quantified as the percentage of the total area per image.

NF-kB transcription factor assay

Nuclear extracts from non-infected and infected cells were prepared using the Nuclear Extraction Kit (Abcam) according to the manufacturer's

instructions. Briefly, cells were trypsinized, centrifuged and resuspended in 1x Pre-Extraction Buffer (100 µl per 1×10^6 cells). After incubation on ice (10 min) and vigorous vortexing, cells were centrifuged (1 min, 12.000 rpm, RT) and the supernatant (cytoplasmic extract) was carefully removed. The Extraction Buffer containing DTT and Protease Inhibitor Cocktail was added to nuclear pellets (10 µl per 1×10^6 cells), extracts were incubated on ice (15 min) and vortexed every 3 min. After centrifugation (10 min, 14.000 rpm, 4 °C), supernatants were transferred into new Eppendorf tubes and stored at −80 °C overnight. On the following day, protein concentrations were adjusted and used for the NF-kB Transcription Factor Assay Kit (Abcam) according to the manufacturer's instructions. Briefly, nuclear extracts were added to a 96-well plate pre-coated with oligonucleotides containing the NF-kB consensus binding site. Wells containing a positive control (Raji nuclear extract with an active NF-kB pathway) and blank wells were included. The plate was incubated for 2.5 h at RT on a rocking platform, washed three times with the Wash Buffer and incubated with 50 µl of the provided primary antibodies (p65 and p50) diluted in the Antibody Binding Buffer at 4 °C overnight, protected from the light. On the following day, the plate was washed as above and incubated with 100 µl of the provided anti-rabbit secondary HRP-antibody (1:1000 dilution in the Antibody Binding Buffer) for 1 h at RT. After washing, the Developing Solution was added (100 µl per well) and the plate was incubated for 5–7 min, protected from the light. The reaction was then stopped with 100 µl of the Stop Solution and the absorbance was measured within 5 min using a FLUOstar OPTIMA (BMG LABTECH, Ortenberg, Germany) spectrophotometer at OD 450 nm with a reference wavelength of OD 665 nm.

Chromatin immunoprecipitation (ChIP) assay

The ChIP assay was performed according to the manufacturer's instructions (Abcam). Briefly, cells were trypsinized, centrifuged and washed with PBS. After centrifugation, cells were resuspended in the fixation buffer containing Buffer A, PBS and formaldehyde at the final concentration of 1.1%. Cells were mixed gently and incubated for 10 min at RT. Glycine was then added (65 µl per 3×10^6 cells) and cells were centrifuged for 5 min at 1.200 rpm at 4 °C. Cells were washed with ice-cold PBS, centrifuged, the supernatant discarded and the pellets were stored at −80 °C overnight. On the next day, chromatin was sonicated and incubated with either the mouse anti-IE72/86 (MAB810R) or a mouse anti-p65 antibody following the manufacturer's instructions for the assay ChIPAb+NFkB p65 (RelA) (Millipore). ChIP primers validated for promoter sequences:

IkB (oligo sequences from Millipore 17-10060 kit)
Forward: 5′-GAC GAC CCC AAT TCA AAT CG-3′
Reverse: TCA GGC TCG GGG AAT TTC C

MIEP (oligo sequences [22])
Forward: GCG GTT TTG GCA GTA CAT CA
Reverse: GGG CGG AGT TGT TAC GAC AT

p21 (oligo sequences [23])
Forward: GTG GCT CTG ATT GGC TTT CTG
Reverse: CTG AAA ACA GGC AGC CCA AG

Chk1 (oligo sequences [23])
Forward: TGG TTC ACA GAA AAA AGG CAA A
Reverse: CGG AGA AAG CGA GCA GTT TAT G

DHFR (oligo sequences)
Forward: TCG CCT GCA CAA ATA GGG AC
Reverse: AGA ACG CGC GGT CAA GTT T

FACS cell cycle analysis

Cells were fixed with 70% cold ethanol and stored at −20 °C for at least 30 min. Cells were then washed with PBS, labeled with 10 µg/ml of propidium iodide (PI) (Invitrogen) containing 5 µg/ml of ribonuclease A (Life Technologies) for 5 min at RT and analyzed on FACSVerse (Becton Dickinson, Franklin Lakes, New Jersey, USA). Staining with the IE72/86 antibody (1 h, RT) and the goat anti-mouse AlexaFluor-488 secondary antibody (1 h, RT) was performed before PI labeling. Acquired data were analyzed using FlowJo software.

DNA fiber assay

Cells were pulse-labeled with 25 µM of CldU (Sigma–Aldrich) for 20 min at 37 °C, washed gently with fresh pre-warmed DMEM and incubated in fresh medium containing 250 µM of IdU (Sigma–Aldrich) for 20 min at 37 °C. Cells were harvested and DNA fibers prepared as described previously [24]. For all experimental conditions, five slides were stretched and two or three slides for each condition were stained. Slides were stored at 4 °C for at least 24 h before being stained. CldU was detected first with a rat anti-BrdU (OBT0030, Serotec) and a DyLight 550 anti-rat (ThermoFisher Scientific) antibodies and IdU was detected with a mouse anti-BrdU (347580, Becton Dickinson) and the AlexaFluor-488 anti-mouse antibodies. Images of well-spread DNA fibers were acquired using the LSM800 confocal microscope, the 63x/1.4 oil immersion objective and LSM ZEN software. Images were acquired semi-automatically by using software autofocus and tile-arrays. Analysis of double-labeled replication forks was performed manually using LSM ZEN software.

Non-denaturing BrdU foci detection

Non-infected and infected cells grown on coverslips were incubated with 10 µM of BrdU (Sigma–Aldrich) for 24 h before being fixed with 4% cold formaldehyde. BrdU was detected using the mouse anti-BrdU and the AlexaFluor-568 anti-mouse antibodies. Images were acquired using the LSM800 confocal microscope, the 63x/1.4 oil immersion objective and LSM ZEN software. Image analysis was performed using ImageJ software.

Cloning and transfection

Cells were transfected with different constructs using the X-tremeGENE 9 DNA Transfection Reagent (Roche) or Lipofectamine 2000 (Invitrogen) according to manufacturers' instructions. The proportion transfection reagent (µl): DNA (µg) was 3:1 for the X-tremeGENE 9 DNA Transfection Reagent and 2.5:1 for Lipofectamine 2000. At 48 h post-transfection, cells were used for the DNA fiber assay, EGFP expression analysis, immunofluorescence or immunoblotting. The following constructs were used: pEGFP-1 (no promoter; Clontech), pCMV-EGFPC1 (CMV promoter; Clontech), pSV40-EGFP-1 (SV40 promoter; Clontech), pSV40-EGFP-LTR-IE72, pIE72-EGFP, pIE86-EGFP and pUL37-EGFP (all created by cloning a relevant sequence into pCMV-EGFPC1).

All polymerase chain reactions (PCR) were carried out with the Q5-polymerase (New England Biolabs, USA). Oligonucleotide synthesis was carried out by IDT (USA). DNA sequencing was carried out by KIgene (Karolinska Institute). Coding sequences for UL37, IE72 and IE86 from HCMV AD169 were cloned into pCMV-EGFPC1 (Clontech) by standard Gibson assembly [25]. All constructs were N-terminally fused to EGFP. All primer sequences are shown in Supplementary Table 1.

Deletion of all 4 binding sites for NF-kB in HCMV MIEP was performed by de novo DNA synthesis. Sequences and plasmids are available upon request.

RT/Q-PCR

RNA was isolated using the RNeasy Mini Kit (Qiagen) and was converted into cDNA using the High Capacity cDNA Reverse Transcription Kit (Applied Biosystems) according to manufacturers' instructions. cDNA was used as a template for Q-PCR with IE72/86 specific primers (TAG Copenhagen): IE72/86 forward 5′-CGA GAC ACC CGT GAC CAA-3′; IE72/86 reverse 5′-CAC TTC ATC TCC TCG AAA GGC-3′; GAPDH forward 5′-TCT CTG CTC CTC CTG TTC GAC-3′; GAPDH reverse 5′-GAC AAG CTT CCC GTT CTC AG-3′. The procedure was performed in the 7300 Real-Time PCR thermocycler (Applied Biosystems) using following parameters: 50 °C for 20 sec, 95 °C for 10 min, then 40 cycles of 95 °C for 15 sec and 60 °C for 1 min. Q-PCR products were verified by agarose gel electrophoresis.

Patient population for immunohistochemistry analysis

This study includes a cohort of glioblastoma multiforme patients treated at the Department of Neurosurgery of the Copenhagen University Hospital (Rigshospitalet) (Supplementary Table 2). Between 2008 and 2014, 20 patients were treated for a newly diagnosed GBM grade IV (WHO 2007 classification). All patients underwent first-time surgical resections combined with the standard temodal/radiation therapy. At a later stage, all patients in the cohort were treated with secondary surgery due to tumor recurrence. Paraffin-embedded archival tissue sections were obtained from all patients from both surgeries. The local ethics committee in Region Hovedstaden approved the study. Since all subjects were deceased, the committee waived the need for informed consent in this study.

Quantification and statistical analysis

Quantitative results are presented as mean values together with the standard deviation from the mean. The choice of the statistical analysis was determined at two levels. If data followed normal Gaussian

distribution, a difference in variances was examined. Data with normal Gaussian distribution and the same variance were analyzed using a parametric unpaired *t* test, while data with normal Gaussian distribution and different variances were analyzed using a parametric *t* test with Welch's correction. If data did not follow normal Gaussian distribution, a non-parametric Kolmogorov-Smirnov test was used.

RESULTS

DDR is functional in HCMV-infected cells

Given the complex relationship between viral infection and host-cell DDR [13, 14, 26], we first directly tested the impact of the virus on responses of human cells to genotoxic insults. We induced different types of DNA lesions at the level that non-infected cells can repair without compromising cell viability (Supplementary Fig. S1A). Human BJ fibroblasts infected with the HCMV strain AD169 were challenged at 48 h post-infection (hpi) for 1 h with 200 ng/ml of the radiomimetic drug neocarzinostatin (NCS), 100 μM of the DNA alkylating agent temozolomide (TMZ) or the inter-strand DNA cross-linker cisplatin (30 μM). All these drugs have been used in the treatment of GBM [27, 28]. Some cells were allowed to recover for 6 h without the drugs and the levels of γH2AX were analyzed by high-throughput microscopy and immunoblotting (Fig. 1A–C and Supplementary Fig. S1B, C, F). Viral infection alone increased both the amount of γH2AX and the number of γH2AX foci, while drug treatment induced and enhanced expression and foci formation of γH2AX in non-infected and infected cells, respectively. After 6 h of recovery, the number of foci and the level of γH2AX remained high selectively in infected cells, indicating a delay in DNA repair. Indeed, DNA repair was delayed in infected cells, as 24 h after NCS treatment the number of γH2AX foci was still elevated (Supplementary Fig. S1B). Next, we examined accumulation of 53BP1, another established marker of DNA repair activity. In infected cells, 53BP1 accumulated gradually around VRC, while another fraction of this otherwise nuclear protein was mislocalized to the cytoplasm. This phenomenon was evident also in cells infected with other HCMV strains: VR1814, Towne and TB40E (Supplementary Fig. S1D, I, J). We quantified the number of 53BP1 foci in each nucleus after drug-induced DNA damage. In untreated infected cells, 53BP1 foci number was already augmented compared to non-infected control cells. After DNA damage and during recovery time, 53BP1 foci were gradually accumulated (Fig. 1D and Supplementary Fig. S1E, G). The cytosolic fraction of 53BP1 was not reduced in response to damage, suggesting it did not shuttle to the nucleus to contribute to DNA repair (Fig. 1E and Supplementary Fig. S1H). These data indicate that HCMV-infected human cells were still able to trigger DDR after exogenous genotoxic insults, albeit with delayed DNA repair kinetics. The aberrant cytosolic DDR protein accumulation after HCMV infection, exemplified here by 53BP1, might reflect aberrantly enhanced expression, a hypothesis we addressed next.

HCMV exploits host-cell stress responses

Earlier work by us and others demonstrated that inflammation, and in particular cytokines TNF-α and IL-6, stimulated HCMV reactivation [29–31]. Through TNF-α mediated NF-kB or via MAPK signaling events and activation of the HCMV major immediate early enhancer and promoter (MIEP) [32], monocytes differentiate into macrophages and reactivate latent HCMV [29]. As analogous studies in response to genotoxic stress are lacking, we next assessed the level of phosphorylated p38 as a marker of MAPK activity after a DNA-damaging insult. As a downstream effector of MAPK signaling, we monitored the level of the transcription factor SP1. As the indication of NF-kB activation, we measured: (i) the level of p65 by immunoblotting (Fig. 2A), (ii) the abundance of nuclear p65 by microscopy (Fig. 2B), and (iii) NF-kB p65 transcription factor DNA binding (Fig. 2C). As expected, the levels of p65 and SP1 were augmented after viral infection. The level of SP1 was further increased when infected cells were treated with NCS or after 6 h of recovery from drug treatment (Fig. 2A). To investigate the effect of DNA damage on the viral protein level and gene expression, we used immunoblotting, high content microscopy and RT/Q-PCR, and analyzed infected cells treated for 1 h with NCS or cisplatin and recovering for 6 h without the drugs. DNA damage enhanced expression of IE72 and IE86 proteins (Fig. 2D–F and Supplementary Fig. S2A–C). Next, we found that NCS induced recruitment of p65 and IE72 to MIEP and increased their binding after 6 h of recovery. In contrast, no differences of p65 recruitment to a control human housekeeping *DHFR* gene promoter were detected upon infection (Fig. 2G, H and Supplementary Fig. S2D, E). We validated our results by transfecting cells with plasmids containing the reporter gene *EGFP* driven by wild-type MIEP, mutated MIEP lacking all 4 NF-kB binding sites or the control SV40 promoter. A construct without any promoter served as a negative control. Treatment with NCS resulted in enhanced expression of EGFP, which was robustly driven only by the wild-type MIEP in both U-2 OS and BJ cells (Fig. 2I and Supplementary Fig. S3A, B). The high level of either IE72/86 or EGFP after NCS treatment could reflect enhanced protein stability or augmented gene expression. We tested the latter possibility by inhibiting two main host-cell RNA polymerases and analyzing IE72/86 expression in infected cells after DNA damage. At the concentration used, actinomycin D (AD) inhibited mainly the activity of RNA pol-I [33], and to inhibit the activity of RNA pol-II, we used the recently developed inhibitor THZ1 [34]. In infected cells treated with NCS, inhibition with THZ1 prevented accumulation of IE72/86, while AD allowed enhanced expression of IE72/86, indicating that RNA pol-II is the main polymerase engaged in augmented gene expression in HCMV-infected cells after DNA damage (Supplementary Fig. S3C). Based on these results, we hypothesized that MIEP might share some features with the promoters of genes involved in host DDR. HCMV MIEP contains binding sites for NF-kB, SP1, AP1 and CREB, among other transcription factors [35]. We analyzed in silico the sequences of promoters of several host genes involved in DDR, most of which turned out to contain transcription-factor binding sites present also in MIEP (Supplementary Fig. S3D, E). To experimentally validate the in silico analysis, we showed that DDR proteins accumulated after infection, whereas the level of housekeeping gene products remained unaffected by the presence of the virus. We included low- and full-serum medium, aphidicolin and γ-irradiation in non-infected cells as controls to monitor the level of host DDR proteins (Supplementary Fig. S4). Additionally, we confirmed the binding of the p65 transcription factor to the promoters of *IκB*, MIEP, *p21* and *Chk1* genes by the ChIP assay (Fig. 2J–M). These results suggest that HCMV MIEP has evolved to exploit the host stress response, as the more stress (here genotoxic) the host experiences, the stronger *IE72/86* genes are expressed.

HCMV evokes replication stress and genomic instability

Gene overexpression, oncogene induction and other factors interfering with cells' replication machinery can cause replication stress (RS) and genomic instability [20, 36]. Because we observed DDR activation and gene overexpression in our experiments, we reasoned that HCMV infection could induce RS with ensuing implications for genomic integrity. As most of the viral genome is replicated 48 hpi and the host's DNA synthesis may not totally be inhibited in infected permissive cells [37, 38], we employed DNA fiber analysis to investigate the effect of viral infection on host DNA synthesis activity at 24 hpi. BJ fibroblasts non-infected or infected with HCMV AD169 were pulse-labeled with CldU for 20 min, washed and pulse-labeled with IdU for subsequent 20 min. The sum of the CldU and IdU pulse length in a DNA fiber measured in μm was then converted into total fork speed in kb/

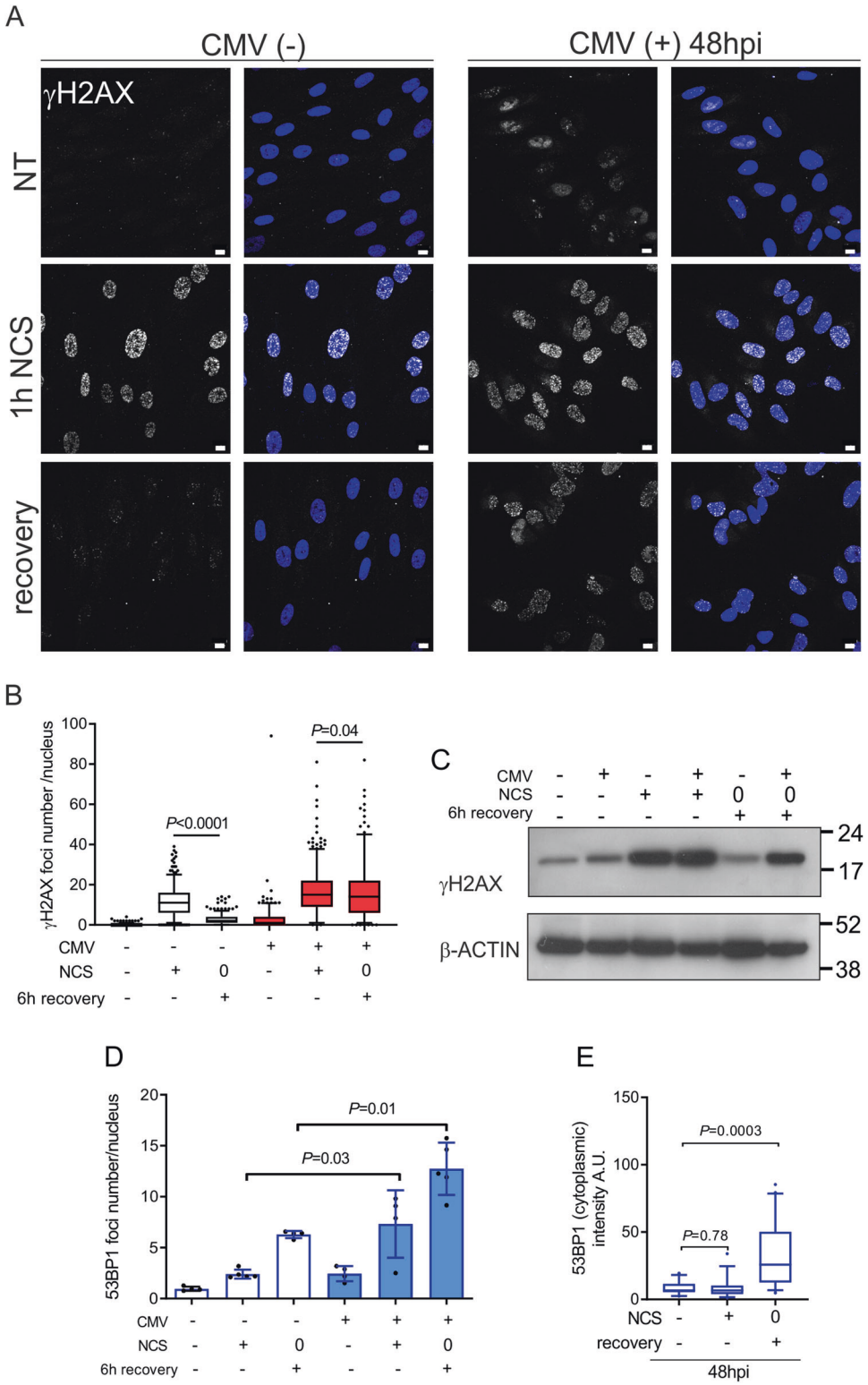

Fig. 1 DDR is functional in HCMV-infected cells. A BJ cells were infected with HCMV AD169 (MOI 3) and 48 hpi were treated with 200 ng/ml of neocarzinostatin (NCS) for 1 h. Cell lysates were then collected or cells were fixed or washed twice with the medium and left for 6 h to recover without NCS. Representative images of γH2AX nuclear immunostaining are shown. **B** The graph shows the mean number of γH2AX foci per nucleus from (**A**). '0' – cells that were treated with the drug for 1 h, washed and left for 6 h to recover without further presence of the drug. **C** Lysates were analyzed for the γH2AX level by immunoblotting. β-actin – loading control. For the uncropped and unmodified Western blots, see Supplemental Material. **D** The graph shows the mean number of 53BP1 foci per nucleus after NCS treatment. **E** The graph shows 53BP1 mean cytoplasmic intensity in BJ fibroblasts 48 hpi with HCMV AD169 (MOI 3) without treatment, after 1 h of NCS or after 6 h of recovery without the drug. Whiskers in box plots indicate the 5–95th percentiles and the center values depict the median. Bar plots show mean ± s.d. Scale bars, 10 μm.

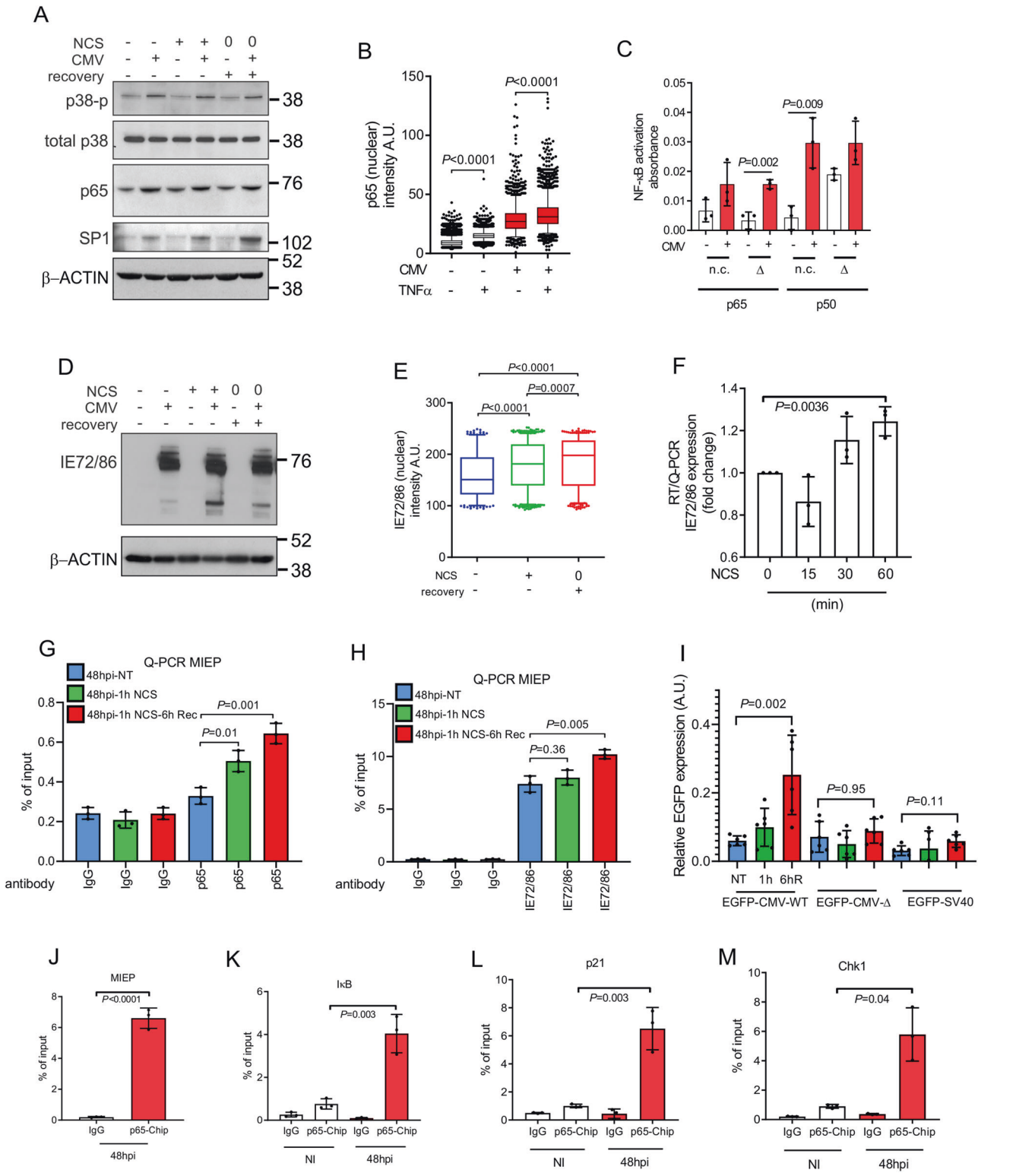

min. Fork asymmetry, as a readout of stalled and collapsed forks, was evaluated by measuring the ratio between the CldU and IdU lengths [39]. Also, to restrict replication fork analysis exclusively to host DNA, we scored only well-isolated forks that were not arranged in tandems and emerged from origins of replication located further than 200 kb apart, as HCMV has only one origin of replication and size of 235 kb. In BJ cells at 24 hpi, fork speed was negatively affected by the presence of the virus. Furthermore, at MOI 10 fork integrity was severely compromised and asymmetric forks were accumulated (Fig. 3A–C and Supplementary Fig. S5A, B).

To further rule out any possibility that our DNA fiber assay in BJ fibroblasts contained active forks from the virus, we searched for a model in which cells can be infected, but replication of HCMV genomes is not supported. We infected several cell lines and quantified the percentage of IE72/86-positive cells at different

Fig. 2 DNA damage induces viral and host protein expression. A BJ cells were infected with HCMV AD169 (MOI 3) and 48 hpi were treated with 200 ng/ml of NCS for 1 h. Cell lysates were collected or cells were washed twice with the medium and left for 6 h to recover without NCS. Lysates were analyzed for phosphorylated-p38, total p38, p65 and SP1 levels by immunoblotting. β-actin – loading control. **B** HCMV-infected BJ fibroblasts were 48 hpi treated with 10 ng/ml of tumor necrosis factor-α (TNF-α) for 30 min. Cells were fixed and analyzed for p65 levels by microscopy. The graph shows p65 mean nuclear intensity. **C** BJ cells were infected with HCMV AD169 (MOI 3) and 48 hpi cell lysates were prepared to test NF-kB activation by a colorimetric assay. Nuclear extracts from non-infected (white bars) and infected (red bars) cells were incubated with the NF-kB consensus binding oligonucleotide and detected with p65 and p50 antibodies. Absorbance values were measured at 450 nm. Experiments were done in triplicates for each condition. A non-competitor (n.c.) oligonucleotide or an NF-kB binding site mutated oligonucleotide (Δ) were added to monitor specificity of the assay. The graph shows activation of NF-kB as indicated by the absorbance level. **D**, **E** HCMV-infected BJ cells treated as in (**A**) were analyzed for IE72/86 levels by immunoblotting (**D**) or microscopy (**E**). β-actin – loading control. The graph shows IE72/86 mean nuclear intensity. **F** HCMV-infected BJ cells were 48 hpi treated with 200 ng/ml of NCS for 15, 30 or 60 min. At all time points, RNA was isolated and RT/Q-PCR with IE72/86 specific primers was performed. The graph shows a fold change in *IE72/86* gene expression. **G**, **H** Chromatin-IP using an IgG isotype control, anti-p65 or anti-IE72/86 antibodies was performed in BJ cells infected and treated as in (**A**). Q-PCR results for the HCMV major immediate early enhancer and promoter (MIEP) region for immune-precipitated DNA are shown. **I** U-2 OS cells were transfected with pEGFP-no promoter, wild-type pEGFP-CMV MIEP (EGFP-CMV-WT), mutated pEGFP-CMV MIEP (EGFP-CMV-Δ) lacking all 4 NF-kB binding sites or pEGFP-SV40 promoter constructs. Cells expressing a plasmid without promoter were used to correct the EGFP background signal. At 48 h post-transfection, cells were treated with 200 ng/ml of NCS for 1 h. Cells were then fixed or washed twice with the medium and left for 6 h to recover without NCS (6hR). Cells were analyzed for EGFP levels by high content microscopy. The graph shows EGFP mean intensity. **J**–**M** BJ cells were infected with HCMV AD169 (MOI 3) and 48 hpi were subjected to ChIP with the p65 specific antibody or an appropriate IgG isotype control. Purified DNA was analyzed by Q-PCR with MIEP (**J**), IκB (**K**), p21 (**L**) or Chk1 (**M**) specific primers for the promoter regions. Graphs show the percentage of ChIP enrichment compared to the input sample from triplicates. Whiskers in box plots indicate the 5–95th percentiles and the center values depict the median. Bar plots show mean ± s.d.

time points post-infection. We found that the osteosarcoma cell line U-2 OS could be infected with HCMV AD169, as cells were able to express IE72/86, but HCMV virions were not produced (Fig. 3D and Supplementary Fig. S5C). The glioblastoma cell line T98G produced some infective viral particles (Fig. 3D and Supplementary Fig. S5C), which is consistent with previous reports [40]. Changes in cell cycle profiles were observed, as U-2 OS infected cells accumulated gradually in G2/M phase, whereas T98G cells resumed a close-to-normal cell cycle profile after a transient peak of G2/M phase-cells at 72 hpi (Supplementary Fig. S5D–F).

Next, we examined the effect of viral infection on genomic DNA synthesis of U-2 OS and T98G cells. As U-2 OS cells cannot sustain viral DNA synthesis, every replication fork must come from host labeled DNA. We found that fork speed was compromised by the presence of active, but not UV-inactivated HCMV AD169 in U-2 OS cells (Fig. 3E and Supplementary Fig. S6D). Moreover, in U-2 OS cells infected with the active virus, accumulation of asymmetric forks occurred (Fig. 3F). Similar results were observed in T98G cells (Supplementary Fig. S6A, B). Consistently with the negative effect on fork integrity, we detected gradual accumulation of single-stranded DNA, γH2AX and 53BP1 foci upon infection (Fig. 3G, H and Supplementary Fig. S6C, E, F). Based on these results we concluded that HCMV AD169 is capable of inducing RS in infected permissive and non-permissive cells. RS can cause genomic instability [41–46], therefore, we analyzed the effect of viral infection on chromosomal integrity of infected cells. We quantified the number of centromeres, a surrogate for the chromosomal ploidy status, in each nucleus of IE72/86-positive U-2 OS and T98G cells at 96 hpi. HCMV infection resulted in accumulation of additional chromosomes in these cells (Supplementary Fig. S7A, B). We also noticed that infected cells accumulated atypical defective mitoses (Fig. 3I, J). The accumulation of atypical defective mitoses was also observed in U-2 OS and T98G cells infected with other HCMV strains: VR1814 at MOI 0.1, 1 and 3 (Supplementary Fig. S7C–E) as well as Towne and TB40E (MOI 3) (Supplementary Fig. S8). Thus, replication stress may contribute to and worsen mitotic defects caused by the dysregulation of the cell cycle machinery in infected cells [47, 48]. We then evaluated whether differences in viral entry [49] and/or viral protein expression could influence the level of replication stress. Consistently across several HCMV strains, cells infected with AD169, Towne or TB40E that expressed IE72/86 accumulated 53BP1 foci (Fig. 4A–C). Interestingly, infection with Towne or TB40E strains increased the number of host-cell asymmetric forks, an established hallmark of replication stress shared also by the AD169 strain, however, the speed of fork progression remained unaffected in Towne- or TB40E-infected cells (Fig. 4D, E). Overall, while all used strains shared the ability to trigger features of replication stress, some differences in the extent of RS caused by different HCMV strains seem to be related to viral infectivity and the resulting level of viral protein expression (Fig. 4F–H), the latter issue addressed also in the next set of experiments. Altogether, we showed that HCMV induces replication stress and exacerbates genomic instability in transformed cells.

To further explore the mechanism behind DNA replication stress in HCMV-infected cells, we sought to determine whether ectopic expression of some of the viral proteins alone induces RS. We transfected U-2 OS cells with different constructs expressing IE72, IE86 or UL37. The expression of the viral mitochondria-localized inhibitor of apoptosis UL37 is not driven by MIEP and it was used as a control (Supplementary Fig. S9A). Notably, expression of either IE72 or IE86, and to a lower extent UL37, decreased the speed of fork progression, affected fork integrity (reflected by enhanced fork asymmetry) and induced accumulation of 53BP1 foci in U-2 OS cells (Fig. 5A–C). Next, we tested more directly whether the level of expressed viral proteins is related to the extent of RS. We focused on the IE72 protein which, unlike the IE86 protein, was previously detected in clinical specimens of human glioblastomas [7], and cloned *IE72* under the control of an LTR sequence, which yields a lower expression of the protein compared with a higher IE72 expression level under the control of MIEP (Supplementary Fig. S9B). The level of IE72 positively correlated with the extent of RS and micronuclei formation, another parameter indicating genomic instability (Fig. 5D–F and Supplementary Fig. S9C–E). These results showed that expression of IE72 and IE86, but not UL37, aggravated genomic instability via replication stress. Altogether, the above data document the dose-dependent biological effects of HCMV infection, its relevance for cells that can survive the infection, and the capacity to trigger replication stress and chromosomal instability.

Radio-chemotherapy insults can activate viral gene expression in tumor cells

Upon experimental HCMV infection of U-2 OS and T98G cells, viral protein expression was gradually silenced in either model. As NCS enhanced IE72/86 expression in BJ fibroblasts, we investigated the effect of this radiomimetic on both infected cancer cell lines. Indeed, when cells at 96 hpi were treated with NCS for 1 h, expression of IE72/86 increased (Fig. 6A–C). Interestingly,

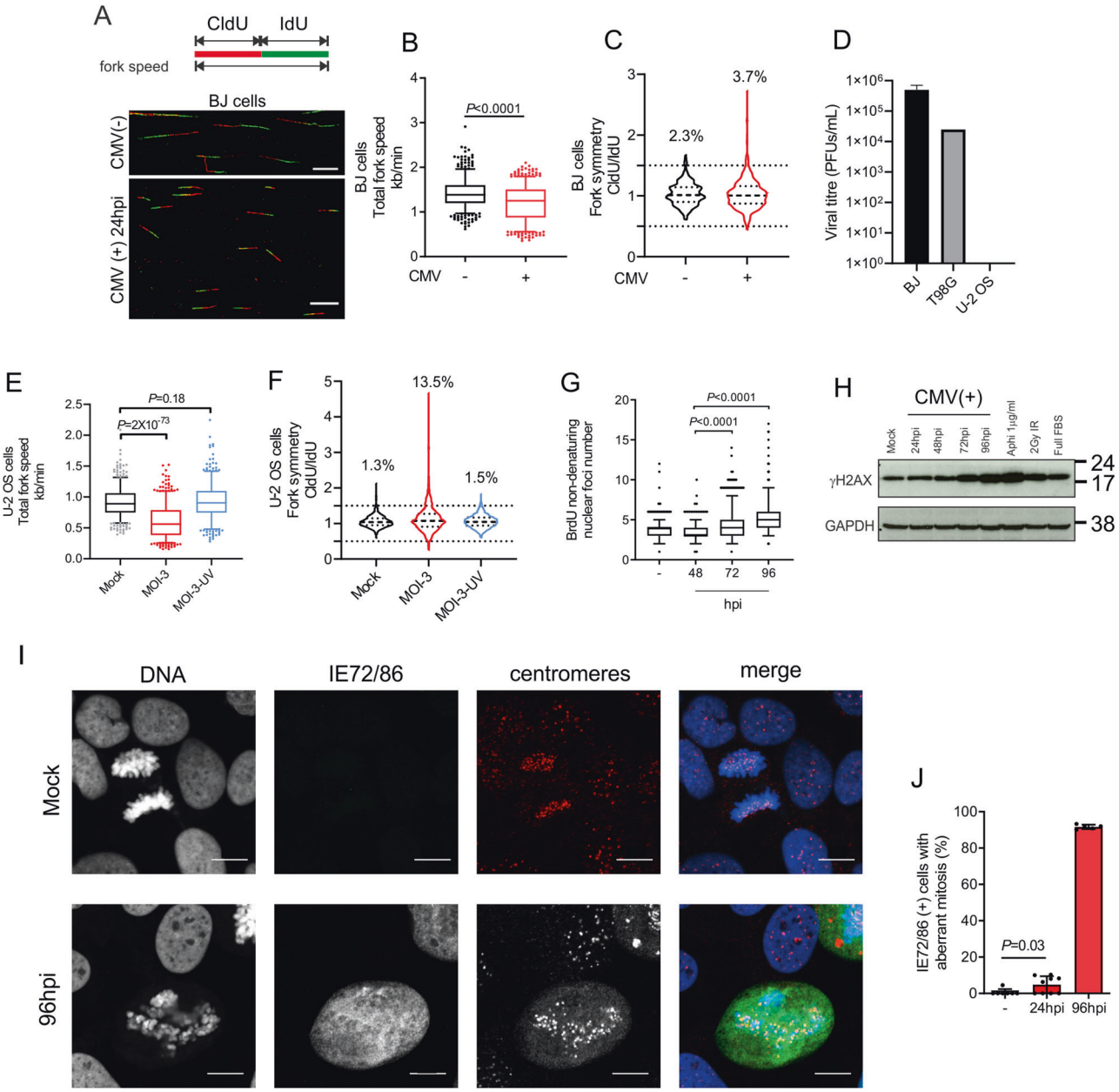

Fig. 3 HCMV AD169 infection triggers replication stress. A A diagram of fork speed analysis and representative images of double-labeled DNA fibers are shown. BJ fibroblasts mock-infected or infected with HCMV AD169 (MOI 3) were 24 hpi pulse-labeled with CldU (red) for 20 min, washed with the medium and pulse-labeled with IdU (green) for subsequent 20 min. Cells were lysed and their DNA stretched. Nucleosides were detected with antibodies and the length of CldU and IdU pulses (μm) was measured separately. **B** The sum of the CldU and IdU pulse length in a DNA fiber from (**A**) was converted into kb/min and is shown as total fork speed. Mean total fork speed: HCMV(−) = 1.4 kb/min and HCMV(+) = 1.2 kb/min; number of scored forks: $n = 588$ and 591, respectively. **C** The ratio of the CldU and IdU pulse length in a DNA fiber was calculated from values in (**B**) to evaluate fork symmetry. Values >1.5 and <0.5 indicate highly asymmetric forks shown as the percentage above each box plot. **D** At 96 hpi supernatants from BJ, T98G and U-2 OS cells infected with HCMV AD169 (MOI 3) were used for the plaque assay. The graph shows the viral titer in PFUs/ml. **E** The graph shows total fork speed (kb/min) in U-2 OS cells mock-infected, infected with HCMV AD169 (MOI 3) or with UV-inactivated HCMV AD169 (MOI 3) 24 hpi. Mean total fork speed: Mock = 0.91 kb/min, MOI-3 = 0.6 kb/min and MOI-3-UV = 0.93 kb/min; number of scored forks: $n = 520$, 538 and 465, respectively. **F** The CldU/IdU ratio was calculated from values in (**E**) to evaluate fork symmetry. **G** U-2 OS cells were infected with HCMV AD169 (MOI 3) and incubated with 10 μM of BrdU for 24 h. At indicated time-points, cells were fixed and BrdU was detected using non-denaturing conditions. **H** U-2 OS cells infected with HCMV AD169 (MOI 3) were analyzed for the γH2AX level at different time post-infection by immunoblotting. GAPDH – loading control. **I** U-2 OS cells were infected with HCMV AD169 (MOI 3) and fixed 96 hpi. An example of aberrant mitosis along with IE72/86 and the centromere marker immunodetection is shown. **J** U-2 OS cells were infected as in (**I**) and aberrant mitosis identified by DNA staining in IE72/86-positive cells 24 and 96 hpi. Whiskers in box plots indicate the 5–95th percentiles and the center values depict the median. Bar plots show mean ± s.d. Scale bars, 10 μm.

glioblastoma T98G cells showed enhanced proliferation when infected with HCMV, while U-2 OS cells proliferated slower when infected (Fig. 6D, E), thereby documenting that responses to HCMV among different cancer cell types might be context-dependent, possibly reflecting the status of their stress-response checkpoint pathways.

Our cell culture mechanistic data indicating enhanced HCMV expression in host cells exposed to genotoxic insults raised the possibility that viral protein expression could be enhanced in human tumor samples after standard-of-care radio-chemotherapy. To test this prediction, we took advantage of the fact that some HCMV proteins can be detected in the majority of human GBM

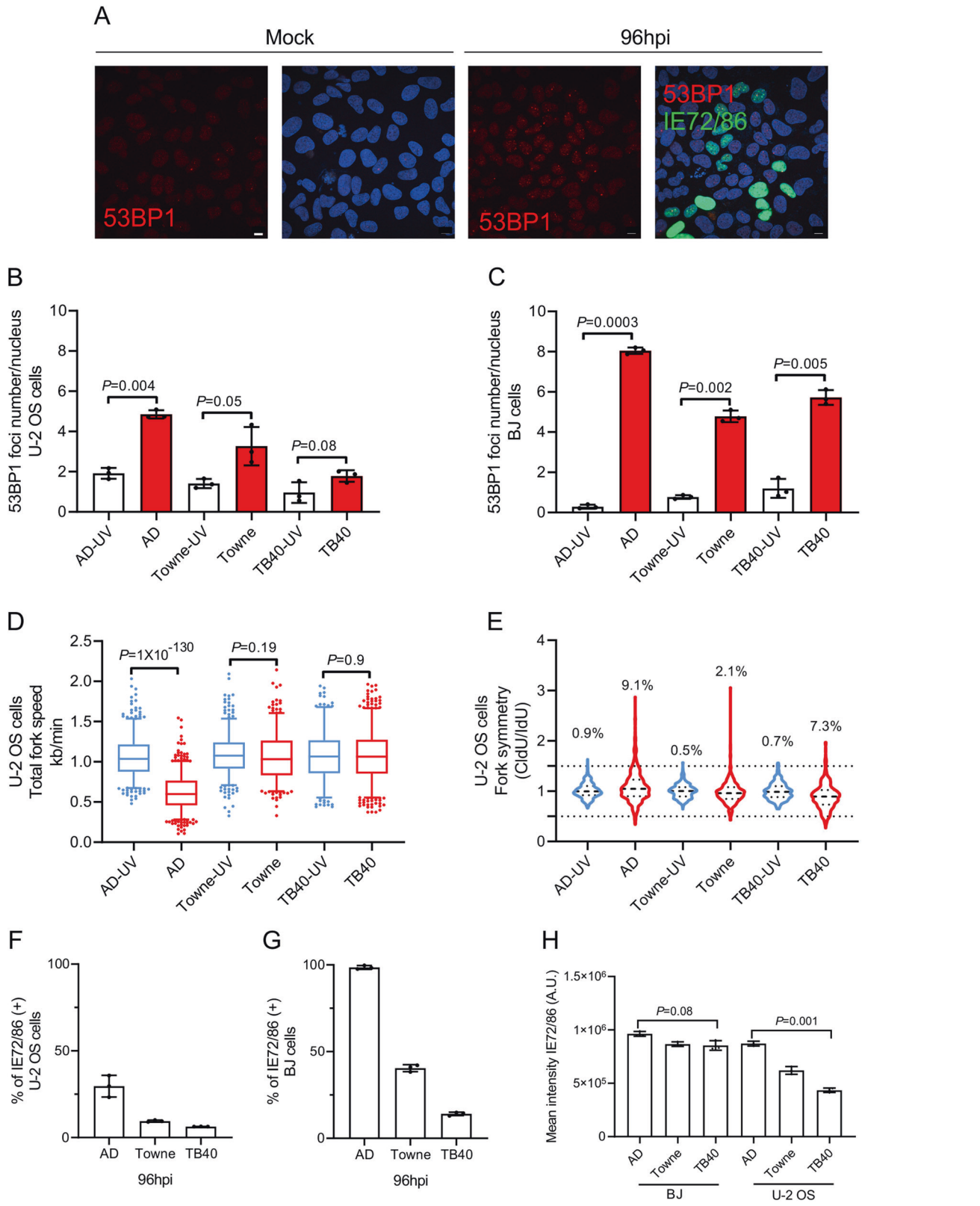

Fig. 4 Replication stress and other HCMV strains. A Representative images of the immunodetection of 53BP1 and IE72/86 proteins in mock-infected or 96hpi U-2 OS cells using the virus strain AD169 at MOI 3 are shown. **B** The graph shows the mean number of 53BP1 foci per nucleus in U-2 OS cells infected with UV-inactivated or infective HCMV viruses at 96 hpi. **C** The same experimental conditions as in (**B**) using BJ cells. Bar plots show mean and S.E.M. **D** U-2 OS cells infected with inactivated (UV) or active viruses were analyzed for DNA fork speed progression by the DNA fiber assay. The graph shows the total fork speed (kb/min). Mean total fork speed: AD169 UV-inactivated (AD-UV) = 1.06 kb/min, AD169 MOI 3 (AD) = 0.62 kb/min, Towne UV-inactivated (Towne-UV) = 1.08 kb/min, Towne MOI 3 (Towne) = 1.06 kb/min, TB40E UV-inactivated (TB40-UV) = 1.07 kb/min, TB40E MOI 3 (TB40) = 1.07 kb/min. Number of scored forks: $n = 468$, 556, 418, 343, 257 and 547, respectively. **E** The CldU/IdU ratio was calculated from values in (**D**) to evaluate fork symmetry. The percentages of highly asymmetric forks are indicated on top of each condition. **F** The graph shows the percentage of IE72/86-positive U-2 OS cells 96hpi with different viral strains (MOI 3). **G** The graph shows the percentage of IE72/86-positive BJ cells 96hpi with different viral strains (MOI 3). **H** The level of IE72/86 expression is shown in cells infected with different viral strains 96hpi. Whiskers in box plots indicate the 5–95th percentiles and the center values depict the median. Bar plots show mean ± s.d (**F**–**H**). Scale bars, 10 μm.

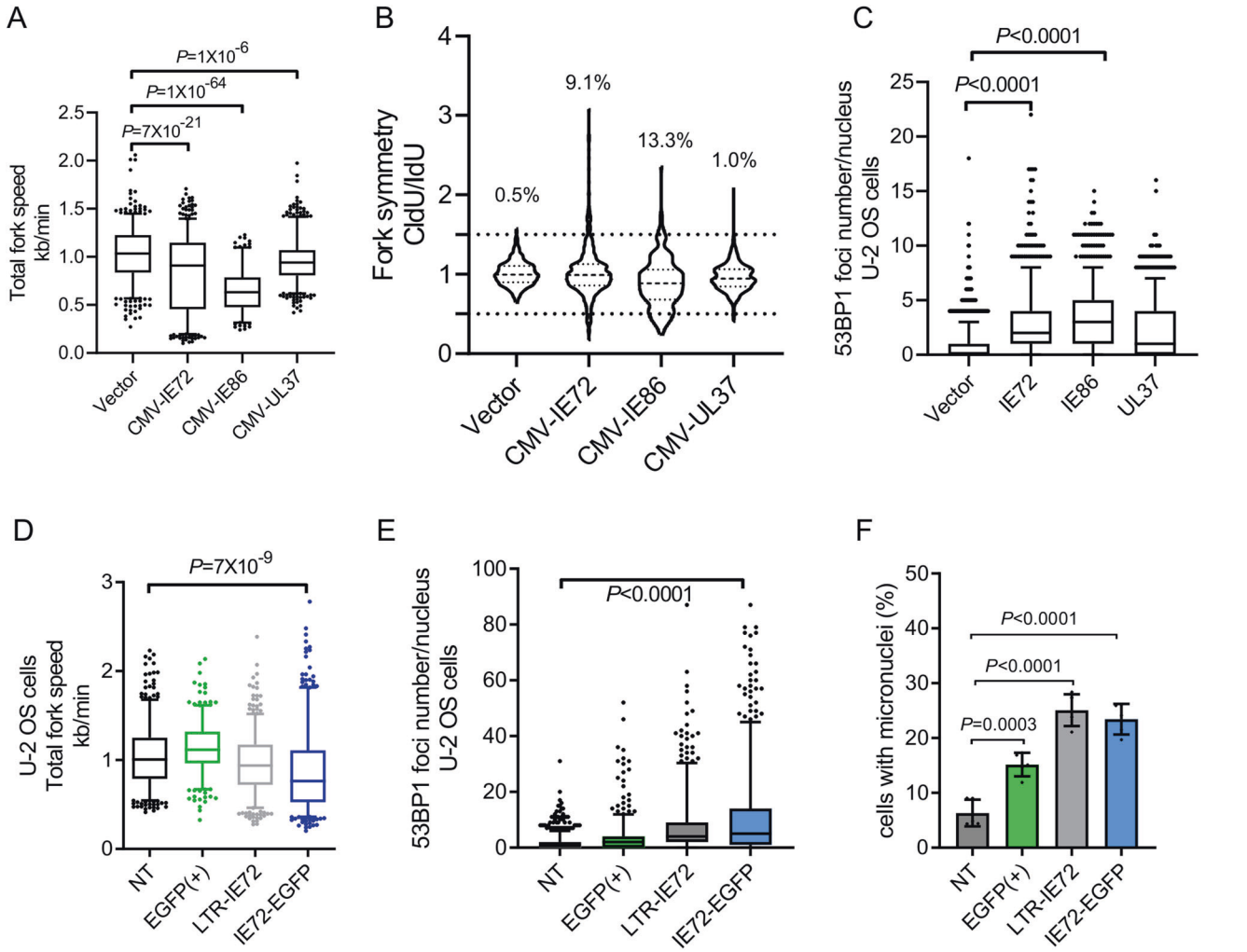

Fig. 5 Ectopic expression of IE72 or IE86 induces replication stress. A U-2 OS cells transfected with an empty vector, pIE72-EGFP, pIE86-EGFP or pUL37-EGFP constructs were 48 h post-transfection analyzed for DNA fork speed progression by the DNA fiber assay. The graph shows the total fork speed (kb/min). Mean total fork speed: empty vector = 1.1 kb/min, IE72 = 0.9 kb/min, IE86 = 0.7 kb/min, UL37 = 1.0 kb/min; number of scored forks: $n = 546$, 535, 217 and 340, respectively. **B** The CldU/IdU ratio was calculated from values in (**A**) to evaluate fork symmetry. (**C**) The graph shows the mean number of 53BP1 foci per nucleus in U-2 OS cells transfected as in (**A**) 48 h post-transfection. **D** U-2 OS cells were transfected with an empty vector (NT), pCMV-EGFPC1 (EGFP(+)), pSV40-EGFP-LTR-IE72 (LTR-IE72) or pCMV-IE72-EGFP (IE72-EGFP) constructs and 48 h post-transfection were analyzed for DNA fork speed progression by the DNA fiber assay. The graph shows the total fork speed (kb/min). Mean total fork speed: NT = 1.04 kb/min, EGFP(+) = 1.14 kb/min, LTR-IE72 = 0.95 kb/min, IE72-EGFP = 0.88 kb/min; number of scored forks: $n = 490$, 340, 476 and 464, respectively. **E** The graph shows the mean number of 53BP1 foci per nucleus in U-2 OS cells transfected as in (**D**) 48 h post-transfection. **F** The graph shows the percentage of U-2 OS cells with micronuclei 48 h post-transfection as in (**D**). Whiskers in box plots indicate the 5–95th percentiles and the center values depict the median. Bar plots show mean ± s.d.

[9, 50] and other brain tumors [26]. We retrieved a panel of tissue biopsies from 20 primary GBM prior to any radio-chemotherapy, and from the matching recurrent lesions of the same patients whose tumor relapsed after treatment (Supplementary Table 2). Quantitative image analysis of tissue sections examined by immunohistochemistry revealed that the protein level of the HCMV IE antigen (detected with the MAB810 ab) was moderately, yet significantly augmented after recurrence, while the HCMV late

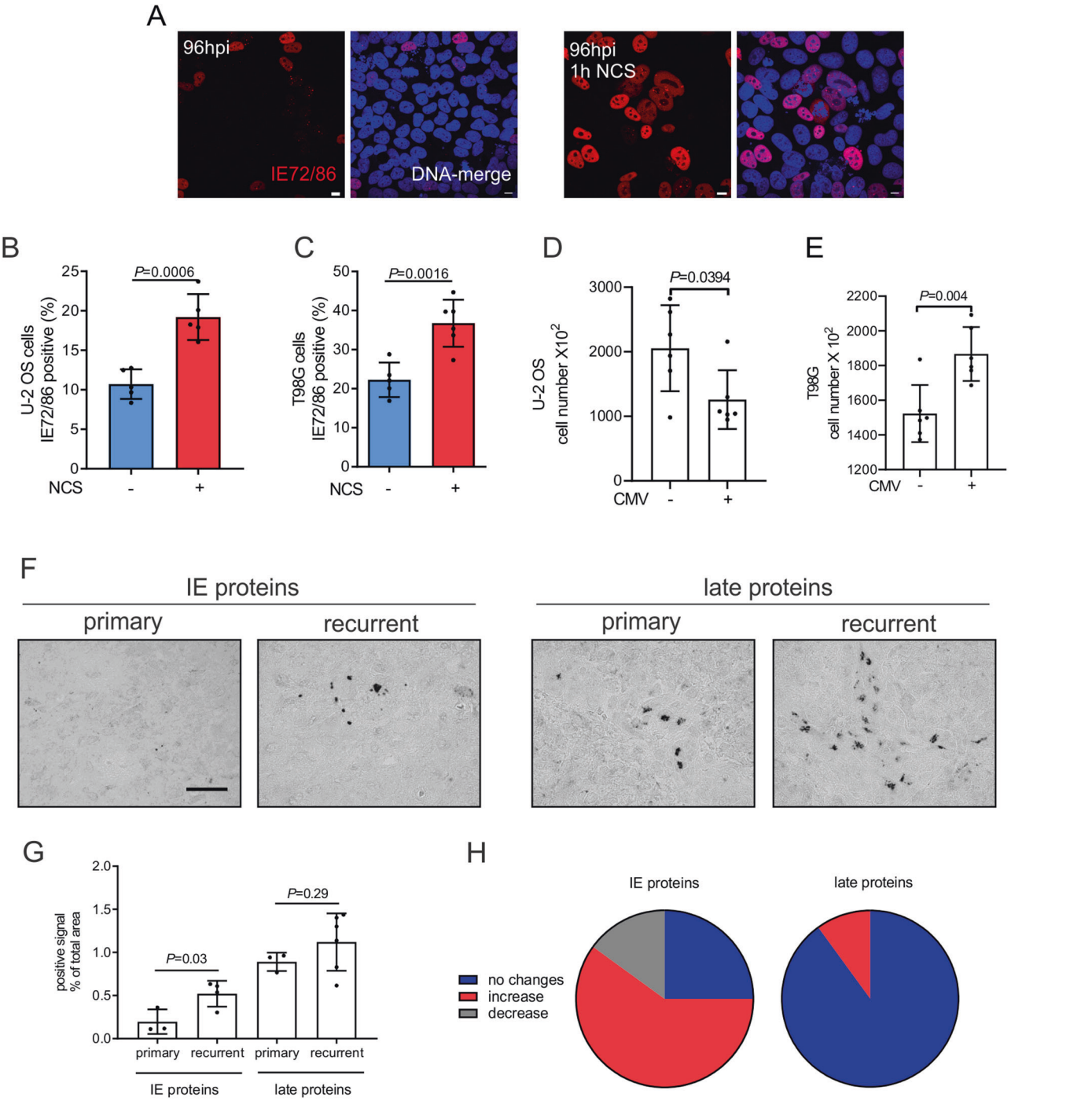

Fig. 6 Exogenous DNA damage reactivates viral protein expression. A U-2 OS cells were infected with HCMV AD169 (MOI 3) and 96 hpi were treated with 200 ng/ml of neocarzinostatin (NCS) for 1 h. Cells were then fixed and immunostained with the IE72/86 antibody. Representative images of IE72/86 (red) immunostaining are shown. Left panel – non-treated cells; right panel – NCS-treated cells. **B**, **C** Graphs show the percentage of IE72/86-positive U-2 OS (**B**) and T98G (**C**) cells 96 hpi with HCMV AD169 (MOI 3) without (blue bars) and with (red bars) NCS treatment (200 ng/ml, 1 h). **D**, **E** Graphs show the total number of U-2 OS (**D**) and T98G (**E**) cells non-infected and 96 hpi with HCMV AD169 (MOI 3). **F** Representative images of immediate early (left panel) and late (right panel) HCMV antigen immunohistochemistry staining of tissue sections from primary and recurrent GBM samples are shown. **G** The graph shows the positive signal of the immediate early and late antigen staining as a percentage of the total area in primary and recurrent GBM tissue samples. **H** Graphs show the pattern of changes in immediate early and late HCMV antigen expression between corresponding primary and recurrent GBM tissue samples ($n = 20$). Bar plots show mean ± s.d. Scale bars, 50 μm (**F**), 10 μm (**A**).

antigen (MAB8127 ab) showed a similar trend, albeit not reaching statistical significance. In addition, a comprehensive semi-quantitative assessment of the percentage of tumor cells expressing HCMV proteins in matched primary and recurrent pairs of tumors from the 20 patients showed that post-treatment recurrent specimens had increased the IE antigen in 60% (12/20) of the matched pairs, in contrast to only 10% matched pairs with a higher late HCMV antigen in recurrence (Fig. 6F–H). While this

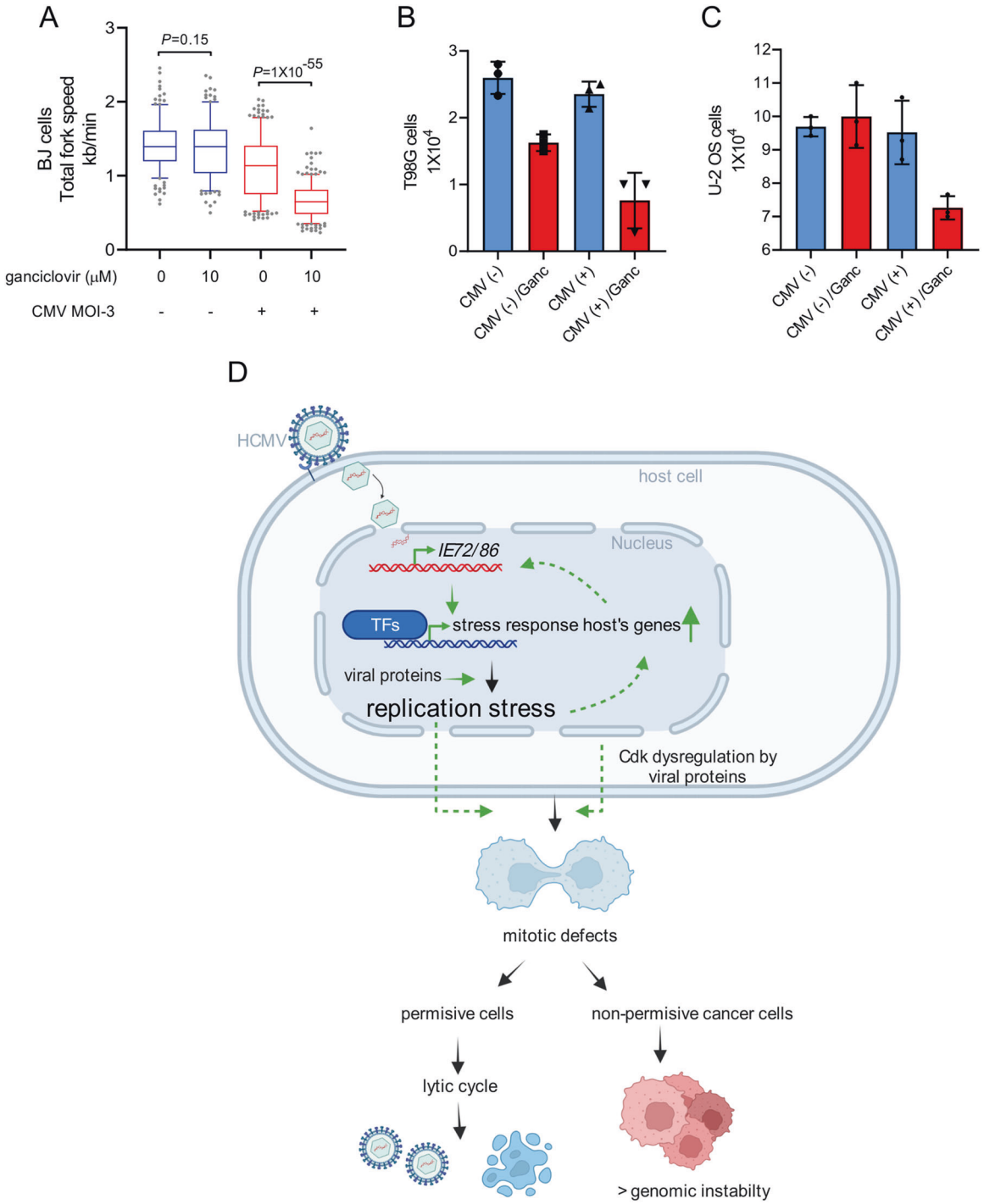

Fig. 7 The effect of ganciclovir on cancer cells. A BJ cells infected with HCMV AD169 (MOI 3) and treated with 10 μM of ganciclovir for 24 h were analyzed for DNA fork speed progression by the DNA fiber assay. The graph shows total fork speed (kb/min). Mean total fork speed: CMV (−) (ganciclovir 0 μM) = 1.4 kb/min, CMV(−) (ganciclovir 10 μM) = 1.37 kb/min, MOI-3 (ganciclovir 0 μM) = 1.1 kb/min and MOI-3 (ganciclovir 10 μM) = 0.66 kb/min; number of scored forks: $n = 254$, 225, 325 and 340, respectively. **B**, **C** T98G and U-2 OS cells were infected with HCMV AD169 (MOI 3) and 24 hpi were treated with 10 μM of ganciclovir for 24 h. Graphs show the total number of T98G (**B**) and U-2 OS (**C**) cells. **D** HCMV-infected cells express IE72 and IE86 viral proteins, which induce expression of transcription factors (TFs) that have binding sites in promoters of other viral genes and host DDR genes. Viral infection induces replication stress and mitotic defects. In permissive cells, HCMV completes its lytic cycle, leading to cell death and the release of competent virions. In non-permissive cells (cancer cells), HCMV infection fuels genomic instability and might increase tumor malignancy. Exogenous transient DNA damage boosts this feedback loop and reactivates IE72/86 expression in cancer cells. BioRender was used to draw the model. Whiskers in box plots indicate the 5–95th percentiles and the center values depict the median. Bar plots show mean ± s.d.

correlation of enhanced HCMV IE protein expression in recurrent, post-treatment clinical tumor specimens cannot be interpreted as proof of causal relationship, these results further support the clinical relevance of HCMV infection, indeed consistent with a possible treatment-evoked HCMV reactivation and its plausible oncomodulatory potential.

Given the above results with recurrent glioblastomas, and our recent report on enhanced survival of human glioblastoma patients treated with an anti-HCMV drug as an add-on to standard radio-chemotherapy [9], we assessed the impact of ganciclovir (GCV) on our experimental models at the host DNA replication level. We found that replication fork integrity in infected BJ fibroblasts was further worsened by ganciclovir treatment (Fig. 7A and Supplementary Fig. S9F). Notably, viability of both cancer cell models, U-2 OS and T98G, was impaired by ganciclovir, selectively in the presence of the virus (Fig. 7B, C). These observations imply that cellular kinases are not sufficient to phosphorylate GCV to its active form to the extent that would induce tumor cell death, and confirm our previous observations that GCV only inhibits tumor growth of HCMV positive tumors [51]. Taken together, our experimental results indicate that ganciclovir may help increase endogenous replication stress in HCMV-infected cancer cells to supra-threshold levels, thereby potentially contributing to the observed therapeutic impact of ganciclovir that is enhanced by the presence of the virus.

DISCUSSION

Considering that HCMV is a globally highly prevalent pathogen [2] whose proteins are commonly found in a wider range of human malignancies [4, 5, 26] than those linked with the papillomaviruses, it is imperative to better understand HCMV's role in tumorigenesis. By examining several complementary models, including also non-permissive human cells capable of surviving infection, we provide insights into three aspects related to HCMV-host interaction in general, and HCMV's emerging involvement in cancer, in particular. First, complementing and extending observations from permissive cells that HCMV can mislocalize the host DDR factors [18], we showed that HCMV does not entirely paralyze, yet delays host DNA repair kinetics. Second, and conceptually more significant, we uncovered an unsuspected mode of how HCMV may hijack and benefit from activated host DDR. Thus, we report that HCMV MIEP contains transcription-factor binding sites shared by promoters of host-cell stress-response genes and, consistently, that experimental DNA damaging insults enhanced IE72/86 expression in non-permissive human cancer cells. Such evolutionary adaptation to mimic host stress-inducible promoters could be advantageous for viral reactivation [52], and may help explain the so-far puzzling phenomenon of HCMV reactivation observed in brain tumor patients undergoing genotoxic therapy [11, 12]. Third, extending the concept of oncogene-evoked replication stress and the ensuing genome instability as a hallmark of cancer [53], we now found that HCMV infection triggers host-cell RS, with detrimental consequences for the fidelity of host DNA replication and genomic (in)stability. HCMV infection resulted in enhanced 53BP1 foci formation, accumulation of single-stranded DNA and asymmetric host DNA replication forks, a bona fide readout of arrested and collapsed forks [39, 44], enhanced frequency of aberrant chromosomal mitotic figures and micronuclei in tumor cells infected with different strains of the virus. The fact that ectopic expression of the HCMV immediate early genes *IE72* and *IE86* may recapitulate induction of RS supports the clinical relevance of our findings, as the IE proteins are commonly detected in human tumor specimens, yet with so far unclarified pathogenic significance [54, 55]. Indeed, host's genomic stability was compromised by ectopic IE72 and IE86 expression, both driven by MIEP. Notably, the extent of RS caused by IE72 is either comparable with (cMyc) or even exceeds (H-Ras) the impact on the same human cells overexpressing active oncogenes, established major triggers of replication stress [41–46] in human malignancies (Supplementary Fig. S9G–J). These unexpected results may help us better understand the largely elusive oncomodulatory role of HCMV in promoting tumorigenesis, as RS is a major mechanism fueling genomic instability in human tumors [53]. Furthermore, patients with HCMV-positive glioblastomas who underwent standard-of-care radio-chemotherapy exhibited elevated HCMV IE72/86 protein levels in post-treatment recurrent tumors, compared with HCMV protein expression in pre-treatment biopsies from the same patient. Thus, radio-chemotherapy through the evoked DDR signaling, in addition to other factors such as therapy-induced inflammation or altered immune response, may contribute to the enhanced expression of viral proteins, which may lead to reactivation of latent virus and poor patient outcome [11, 12]. These results are consistent with our proposed concept of MIEP hijacking transcription-factor binding sites shared with host stress-response genes. Our data support recent promising reports of the beneficial outcome of treatment with valganciclovir [56] and HCMV vaccines [57] in patients with GBM, and may help explain recent observations of HCMV reactivation and encephalitis in a substantial proportion of brain tumor patients after radio-chemotherapy. Based on our results, we propose a model to explain a likely major aspect of the oncomodulatory effects of HCMV through induction of replication stress, subversion of host's DDR machinery and genomic instability (Fig. 7D). Overall, our mechanistic model could inspire future strategies to combine radio-chemotherapy with repurposing of anti-viral drugs for cancer treatment, a notion currently under evaluation in our ongoing double-blind placebo-controlled clinical trial VIGAS2 (ClinicalTrials.gov Identifier: NCT04116411).

DATA AVAILABILITY

Constructs, maps, sequences and any other raw data supporting the present study are available upon request to any of the corresponding authors.

REFERENCES

1. de Martel C, Georges D, Bray F, Ferlay J, Clifford GM. Global burden of cancer attributable to infections in 2018: a worldwide incidence analysis. Lancet Glob Health. 2020;8:e180–e90.
2. Zuhair M, Smit GSA, Wallis G, Jabbar F, Smith C, Devleesschauwer B, et al. Estimation of the worldwide seroprevalence of cytomegalovirus: a systematic review and meta-analysis. Rev Med Virol. 2019;29:e2034.
3. Rawlinson WD, Hamilton ST, van Zuylen WJ. Update on treatment of cytomegalovirus infection in pregnancy and of the newborn with congenital cytomegalovirus. Curr Opin Infect Dis. 2016;29:615–24.
4. Harkins LE, Matlaf LA, Soroceanu L, Klemm K, Britt WJ, Wang W, et al. Detection of human cytomegalovirus in normal and neoplastic breast epithelium. Herpesviridae.2010;1:8.
5. Boldogh I, Baskar JF, Mar EC, Huang ES. Human cytomegalovirus and herpes simplex type 2 virus in normal and adenocarcinomatous prostate glands. J Natl Cancer Inst. 1983;70:819–26.
6. Soroceanu L, Matlaf L, Bezrookove V, Harkins L, Martinez R, Greene M, et al. Human cytomegalovirus US28 found in glioblastoma promotes an invasive and angiogenic phenotype. Cancer Res. 2011;71:6643–53.
7. Bhattacharjee B, Renzette N, Kowalik TF. Genetic analysis of cytomegalovirus in malignant gliomas. J Virol. 2012;86:6815–24.
8. Cobbs CS, Harkins L, Samanta M, Gillespie GY, Bharara S, King PH, et al. Human cytomegalovirus infection and expression in human malignant glioma. Cancer Res. 2002;62:3347–50.
9. Soderberg-Naucler C, Rahbar A, Stragliotto G. Survival in patients with glioblastoma receiving valganciclovir. N Engl J Med. 2013;369:985–6.
10. Schuessler A, Smith C, Beagley L, Boyle GM, Rehan S, Matthews K, et al. Autologous T-cell therapy for cytomegalovirus as a consolidative treatment for recurrent glioblastoma. Cancer Res. 2014;74:3466–76.
11. Goerig NL, Frey B, Korn K, Fleckenstein B, Uberla K, Schmidt MA, et al. Frequent occurrence of therapeutically reversible CMV-associated encephalopathy during radiotherapy of the brain. Neuro Oncol. 2016;18:1664–72.

12. Goerig NL, Frey B, Korn K, Fleckenstein B, Uberla K, Schmidt MA, et al. Early mortality of brain cancer patients and its connection to cytomegalovirus reactivation during radiochemotherapy. Clin Cancer Res. 2020;26:3259–70.
13. Luo MH, Rosenke K, Czornak K, Fortunato EA. Human cytomegalovirus disrupts both ataxia telangiectasia mutated protein (ATM)- and ATM-Rad3-related kinase-mediated DNA damage responses during lytic infection. J Virol. 2007;81:1934–50.
14. Xiaofei E, Kowalik TF. The DNA damage response induced by infection with human cytomegalovirus and other viruses. Viruses.2014;6:2155–85.
15. E X, Pickering MT, Debatis M, Castillo J, Lagadinos A, Wang S, et al. An E2F1-mediated DNA damage response contributes to the replication of human cytomegalovirus. PLoS Pathog. 2011;7:e1001342.
16. E X, Savidis G, Chin CR, Wang S, Lu S, Brass AL, et al. A novel DDB2-ATM feedback loop regulates human cytomegalovirus replication. J Virol. 2014;88:2279–90.
17. Zavala AG, O'Dowd JM, Fortunato EA. Infection of a single cell line with distinct strains of human cytomegalovirus can result in large variations in virion production and facilitate efficient screening of virus protein function. J Virol. 2015;90:2523–35.
18. Gaspar M, Shenk T. Human cytomegalovirus inhibits a DNA damage response by mislocalizing checkpoint proteins. Proc Natl Acad Sci USA. 2006;103:2821–6.
19. O'Dowd JM, Zavala AG, Brown CJ, Mori T, Fortunato EA. HCMV-infected cells maintain efficient nucleotide excision repair of the viral genome while abrogating repair of the host genome. PLoS Pathog. 2012;8:e1003038.
20. Maya-Mendoza A, Ostrakova J, Kosar M, Hall A, Duskova P, Mistrik M, et al. Myc and Ras oncogenes engage different energy metabolism programs and evoke distinct patterns of oxidative and DNA replication stress. Mol Oncol. 2015;9:601–16.
21. Bartkova J, Bakkenist CJ, Rajpert-De Meyts E, Skakkebaek NE, Sehested M, Lukas J, et al. ATM activation in normal human tissues and testicular cancer. Cell Cycle. 2005;4:838–45.
22. Ma AN, Wang H, Guo R, Wang YX, Li W, Cui J, et al. Targeted gene suppression by inducing de novo DNA methylation in the gene promoter. Epigenetics Chromatin. 2014;7:20.
23. Jackson JG, Pereira-Smith OM. p53 is preferentially recruited to the promoters of growth arrest genes p21 and GADD45 during replicative senescence of normal human fibroblasts. Cancer Res. 2006;66:8356–60.
24. Maya-Mendoza A, Olivares-Chauvet P, Kohlmeier F, Jackson DA. Visualising chromosomal replication sites and replicons in mammalian cells. Methods.2012;57:140–8.
25. Gibson DG, Young L, Chuang RY, Venter JC, Hutchison CA 3rd, Smith HO. Enzymatic assembly of DNA molecules up to several hundred kilobases. Nat Methods. 2009;6:343–5.
26. Bartek J, Jr. Fornara O, Merchut-Maya JM, Maya-Mendoza A, Rahbar A, Stragliotto G, et al. Replication stress, DNA damage signalling, and cytomegalovirus infection in human medulloblastomas. Mol Oncol. 2017;11:945–64.
27. Brandes AA, Basso U, Reni M, Vastola F, Tosoni A, Cavallo G, et al. First-line chemotherapy with cisplatin plus fractionated temozolomide in recurrent glioblastoma multiforme: a phase II study of the Gruppo Italiano Cooperativo di Neuro-Oncologia. J Clin Oncol. 2004;22:1598–604.
28. Uemura S, Matsukado Y, Kuratsu J, Sonoda H, Ohtsuka T, Yoshioka S, et al. [Local chemotherapy of malignant glioma. Intra-tumoral administration of neocarzinostatin]. Neurol Med Chir (Tokyo). 1986;26:468–74.
29. Soderberg-Naucler C, Fish KN, Nelson JA. Reactivation of latent human cytomegalovirus by allogeneic stimulation of blood cells from healthy donors. Cell .1997;91:119–26.
30. Reeves M, Sissons P, Sinclair J. Reactivation of human cytomegalovirus in dendritic cells. Disco Med. 2005;5:170–4.
31. Reeves MB, Compton T. Inhibition of inflammatory interleukin-6 activity via extracellular signal-regulated kinase-mitogen-activated protein kinase signaling antagonizes human cytomegalovirus reactivation from dendritic cells. J Virol. 2011;85:12750–8.
32. Stein J, Volk HD, Liebenthal C, Kruger DH, Prosch S. Tumour necrosis factor alpha stimulates the activity of the human cytomegalovirus major immediate early enhancer/promoter in immature monocytic cells. J Gen Virol. 1993;74:2333–8.
33. Martin C, Chen S, Maya-Mendoza A, Lovric J, Sims PF, Jackson DA. Lamin B1 maintains the functional plasticity of nucleoli. J Cell Sci. 2009;122:1551–62.
34. Kwiatkowski N, Zhang T, Rahl PB, Abraham BJ, Reddy J, Ficarro SB, et al. Targeting transcription regulation in cancer with a covalent CDK7 inhibitor. Nature.2014;511:616–20.
35. Stinski MF, Isomura H. Role of the cytomegalovirus major immediate early enhancer in acute infection and reactivation from latency. Med Microbiol Immunol. 2008;197:223–31.
36. Costantino L, Sotiriou SK, Rantala JK, Magin S, Mladenov E, Helleday T, et al. Break-induced replication repair of damaged forks induces genomic duplications in human cells. Science.2014;343:88–91.
37. DeMarchi JM, Kaplan AS. Replication of human cytomegalovirus DNA: lack of dependence on cell DNA synthesis. J Virol. 1976;18:1063–70.
38. Yamanishi K, Fogel M, Rapp F. Effect of caffeine on the replication of non-irradiated and ultraviolet-irradiated cytomegalovirus. Intervirology.1978;10:241–53.
39. Maya-Mendoza A, Moudry P, Merchut-Maya JM, Lee M, Strauss R, Bartek J. High speed of fork progression induces DNA replication stress and genomic instability. Nature.2018;559:279–84.
40. Luo MH, Fortunato EA. Long-term infection and shedding of human cytomegalovirus in T98G glioblastoma cells. J Virol. 2007;81:10424–36.
41. Halazonetis TD, Gorgoulis VG, Bartek J. An oncogene-induced DNA damage model for cancer development. Science.2008;319:1352–5.
42. Bartkova J, Horejsi Z, Koed K, Kramer A, Tort F, Zieger K, et al. DNA damage response as a candidate anti-cancer barrier in early human tumorigenesis. Nature.2005;434:864–70.
43. Gorgoulis VG, Vassiliou LV, Karakaidos P, Zacharatos P, Kotsinas A, Liloglou T, et al. Activation of the DNA damage checkpoint and genomic instability in human precancerous lesions. Nature.2005;434:907–13.
44. Burrell RA, McClelland SE, Endesfelder D, Groth P, Weller MC, Shaikh N, et al. Replication stress links structural and numerical cancer chromosomal instability. Nature.2013;494:492–6.
45. Maiani E, Milletti G, Nazio F, Holdgaard SG, Bartkova J, Rizza S, et al. AMBRA1 regulates cyclin D to guard S-phase entry and genomic integrity. Nature.2021;592:799–803.
46. Venkatesan S, Angelova M, Puttick C, Zhai H, Caswell DR, Lu WT, et al. Induction of APOBEC3 exacerbates DNA replication stress and chromosomal instability in early breast and lung cancer evolution. Cancer Disco. 2021;11:2456–73.
47. Hertel L, Chou S, Mocarski ES. Viral and cell cycle-regulated kinases in cytomegalovirus-induced pseudomitosis and replication. PLoS Pathog. 2007;3:e6.
48. Hertel L, Mocarski ES. Global analysis of host cell gene expression late during cytomegalovirus infection reveals extensive dysregulation of cell cycle gene expression and induction of Pseudomitosis independent of US28 function. J Virol. 2004;78:11988–2011.
49. Tang J, Frascaroli G, Lebbink RJ, Ostermann E, Brune W. Human cytomegalovirus glycoprotein B variants affect viral entry, cell fusion, and genome stability. Proc Natl Acad Sci USA. 2019;116:18021–30.
50. Wolmer-Solberg N, Baryawno N, Rahbar A, Fuchs D, Odeberg J, Taher C, et al. Frequent detection of human cytomegalovirus in neuroblastoma: a novel therapeutic target? Int J Cancer. 2013;133:2351–61.
51. Baryawno N, Rahbar A, Wolmer-Solberg N, Taher C, Odeberg J, Darabi A, et al. Detection of human cytomegalovirus in medulloblastomas reveals a potential therapeutic target. J Clin Invest. 2011;121:4043–55.
52. Traylen CM, Patel HR, Fondaw W, Mahatme S, Williams JF, Walker LR, et al. Virus reactivation: a panoramic view in human infections. Future Virol. 2011;6:451–63.
53. Macheret M, Halazonetis TD. DNA replication stress as a hallmark of cancer. Annu Rev Pathol. 2015;10:425–48.
54. Shen Y, Zhu H, Shenk T. Human cytomagalovirus IE1 and IE2 proteins are mutagenic and mediate "hit-and-run" oncogenic transformation in cooperation with the adenovirus E1A proteins. Proc Natl Acad Sci USA. 1997;94:3341–5.
55. Doniger J, Muralidhar S, Rosenthal LJ. Human cytomegalovirus and human herpesvirus 6 genes that transform and transactivate. Clin Microbiol Rev. 1999;12:367–82.
56. Stragliotto G, Pantalone MR, Rahbar A, Bartek J, Soderberg-Naucler C. Valganciclovir as Add-on to standard therapy in glioblastoma patients. Clin Cancer Res. 2020;26:4031–9.
57. Schuessler A, Walker DG, Khanna R. Cytomegalovirus as a novel target for immunotherapy of glioblastoma multiforme. Front Oncol. 2014;4:275.

ACKNOWLEDGEMENTS

We acknowledge the support of Christoffel Dinant and the BioImaging Core Facility at the Danish Cancer Society Research Center.

AUTHOR CONTRIBUTIONS

JMM-M, AM-M, CS-N and JB conceived the study and designed experiments. JMM-M, AM-M, JBjr, Jirina B, PG, MHL, HLC, PJS and MRP performed experiments. JMM-M, JBjr, PG, HLC, PJS, CBB, HB, Jirina B, MRP, CS-N, JB and AM-M analyzed and interpreted the data. JMM-M, AM-M, CS-N and JB wrote the manuscript.

FUNDING

This work was supported by grants from The Danish Cancer Society (# R1123-A7785-15-S2, R167-A11068), The Lundbeck Foundation (R266-2017-4289, R322-2019-2577),

The Danish Council for Independent Research (# DFF-7016-00313), The Novo Nordisk Foundation (grant # 0060590), The Swedish Research Council VR-MH 2014-46602-117891-30, The Swedish Cancer Foundation/Cancerfonden (# 170176), Swedish Medical Research Council (2019-01736), The Danish National Research Foundation (project CARD, DNRF 125), Grant Agency of the Czech Ministry of Health (NU21-03-00195), Family Ehrling Persson´s Foundation, Sten A Olssons Foundation, BILTEMA Foundation and Family of Jochnich´s Foundation.

COMPETING INTERESTS

The authors declare no competing interests.

ETHICS APPROVAL AND CONSENT TO PARTICIPATE

The study was performed in accordance with the Declaration of Helsinki. Our study includes a cohort of glioblastoma multiforme patients treated at the Department of Neurosurgery of the Copenhagen University Hospital (Rigshospitalet) between 2008 and 2014. The local ethics committee in Region Hovedstaden approved the study. Since all subjects were deceased, the committee waived the need for informed consent in this study.

ADDITIONAL INFORMATION

Supplementary information The online version contains supplementary material available at https://doi.org/10.1038/s41418-022-00953-w.

Correspondence and requests for materials should be addressed to Apolinar Maya-Mendoza, Cecilia Söderberg-Naucler or Jiri Bartek.